SOFT MATERIALS
2023, VOL. 21, NO. 1, 14–22
https://doi.org/10.1080/1539445X.2022.2115514

Taylor & Francis
Taylor & Francis Group

Lateral response of a layered material with interlayer friction

Tomoki Sasada[a*], Kento Yasuda[b*], Yuto Hosaka[c], and Shigeyuki Komura[a,d,e]

[a]Department of Chemistry, Graduate School of Science, Tokyo Metropolitan University, Tokyo, Japan; [b]Research Institute for Mathematical Sciences, Kyoto University, Kyoto, Japan; [c]Max Planck Institute for Dynamics and Self-Organization (MPI DS), Göttingen, Germany; [d]Wenzhou Institute, University of Chinese Academy of Sciences, Wenzhou, Zhejiang, China; [e]Oujiang Laboratory, Wenzhou, Zhejiang, China

ABSTRACT

We investigate the mechanical properties of a layered material with interlayer friction. We propose a model that contains lateral elasticity and interlayer friction to obtain the response function both in the Fourier and real spaces. By investigating how the internal deformation is laterally induced due to the applied surface displacement, we find that it is transmitted into the material with an apparent phase difference. We also obtain the effective complex modulus of the layered material and show that it exhibits an intermediate power-law behavior in the low-frequency regime. Our results can be used to estimate the internal deformation of layered materials that exists on various different scales.

ARTICLE HISTORY
Received 9 May 2022
Accepted 17 August 2022

KEYWORDS
Layer; lamellar; smectic; viscoelastic; rheology

Introduction

Although the rheology of soft materials is an important subject, their nonlinear viscoelasticity as well as linear viscoelastic behaviors are not fully understood. For a structurally homogeneous material, the linear viscoelasticity can be characterized by the frequency-dependent complex modulus $G^*(\omega)$. Typical soft materials, however, contain mesoscopic internal structures that can deform under weak external fields, leading to unique viscoelastic behaviors.[1,2] These internal structures play essential roles for the mechanical response at low-frequencies, whereas the molecular interactions control the high-frequency response. To describe the internal mesoscopic structures of soft materials, a coupling mechanism between elastic and viscous components have often been considered. In the two-fluid model for a polymer gel, for instance, the consisting polymer network is represented by an elastic material and the solvent is described as a viscous fluid.[3,4]

The mechanical response of a layered material such as the smectic phase in liquid crystals[5–10] or the lamellar phase in diblock copolymers.[11] In the experiments, the orientation of the stacked layers can be controlled by various methods. For example, the lamellar structure in block copolymers can be oriented in the flow direction under a weak shear flow, while it becomes perpendicular to the flow for a strong shear flow.[11] To explain the anomalous frequency dependence of the complex modulus of the lamellar structure in block copolymers,[11–14] Kawasaki and Onuki considered the coupling between the bending elasticity of the lamellar layers and the viscosity of the surrounding fluid.[15]

Layered structures exist not only in soft materials but also in biological materials, hard condensed matter, and in the field of geology. The corresponding examples are epithelial tissues,[16] graphene sheets,[17,18] layered viscoelastic materials,[19] and geological strata, respectively. However, a general model to describe such a layered structure has not yet been considered.

In this paper, we propose a continuum model for an oriented layered material that contains lateral elasticity and interlayer friction to investigate its mechanical properties. In our model, each layer is described as a two-dimensional (2D) elastic sheet that undergoes both shear and areal deformations. The frictional interaction between the layers is phenomenologically introduced through the velocity gradient of the layers. Due to this coupling effect, the overall mechanical response becomes viscoelastic and frequency-dependent. Considering only the in-plane deformation, we obtain the response function that relates the surface displacement to the internal deformation both in the Fourier space and real spaces. We examine how the surface lateral displacement is transmitted into the material as a function of the depth or the distance. Moreover, we shall obtain the effective complex modulus of the layered material and discuss its asymptotic behaviors.

CONTACT Shigeyuki Komura komura@wiucas.ac.cn Wenzhou Institute, University of Chinese Academy of Sciences, Wenzhou, Zhejiang 325001, China
*These authors contributed equally to this work.

Before presenting our model, we shall clarify the differences between fluid membranes and elastic sheets. Previously, both the static and dynamic properties of a stack of fluid membranes or the lamellar phase in lyotropic liquid crystals were studied experimentally and theoretically.[20–22] In particular, the shear-induced transition from the lamellar phase to the onion phase in lyotropic systems was investigated.[23–27] The deformation of a fluid membrane is described by its out-of-plane displacement because it is incompressible and there is no restoring force against shear deformation. For an elastic sheet, however, the in-plane and out-of-plane displacements are coupled to each other in a nonlinear manner, and its deformation is highly nontrivial.[28–30] This is one of the reasons that we limit our analysis only to the in-plane lateral response, and further discussion concerning the extension of our work will be given in the last section.

For a fluid membrane which has two-dimensional shear viscosity, the inter-leaflet friction between two monolayers in a bilayer membrane is recognized as another source of dissipation.[31–34] Such friction arises due to the velocity difference between the upper and lower leaflets of the bilayer. However, the interlayer friction between elastic sheets was not considered before, and we shall propose the simplest continuum model to take into account such an effect.

In Section II, we describe our continuum model for a layered material with interlayer friction. In Sections III and IV, we obtain the response functions in the Fourier and the real spaces, respectively, and further discuss the longitudinal and transverse responses. The effective complex modulus of a layered material is calculated in Section. V. Finally, a summary and some further discussion are given in Section VI.

Model of a Layered Material

We first discuss the stress tensor of a 2D elastic sheet that comprises the layered material as shown in Figure 1 where the layers are stacked in the z-direction. We introduce the time-dependent 2D lateral in-plane displacement field $\mathbf{u}(\mathbf{r}, z, t) = (u_x(\mathbf{r}, z, t), u_y(\mathbf{r}, z, t))$ where $\mathbf{r} = (x, y)$ is the 2D coordinate. In this work, we do not consider any out-of-plane deformation of the sheet. Then the strain tensor can be defined by

$$\varepsilon_{ij} = \frac{1}{2}\left(\partial_i u_j + \partial_j u_i\right), \tag{1}$$

where $i, j = x, y$. Within the linear elasticity theory, the 2D stress tensor is related to the above strain tensor by the Hook's law[28]

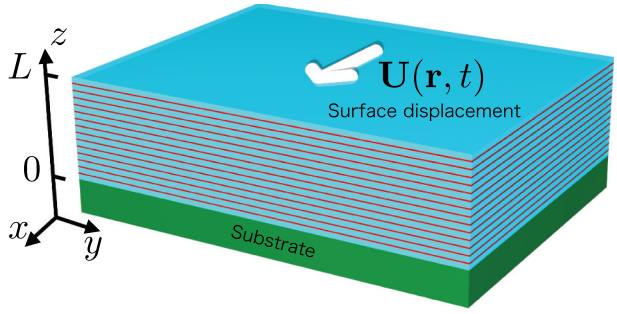

Figure 1. Layered material of thickness L consisting of two-dimensional elastic sheets (red layers) and thin fluid (blue layers). The surface displacement $\mathbf{U}(\mathbf{r}, t)$ at $z = L$ propagates into the material. The layered material is supported by a solid substrate at $z = 0$ where the deformation vanishes.

$$\sigma_{ij} = \lambda \varepsilon_{kk}\delta_{ij} + 2\mu\varepsilon_{ij}, \tag{2}$$

where δ_{ij} is the Kronecker delta, λ and μ are the 2D Lamé coefficients, and the summation over repeated indices is implicitly assumed. Here, the symmetry $\sigma_{ij} = \sigma_{ji}$ implies the 2D isotropy of the elastic sheet.

To characterize the layered structure, we consider frictional forces acting between the elastic sheets. In the small displacement limit, the frictional force is proportional to the velocity difference between the two neighboring sheets. When the thickness of each layer h is small enough, the stress acting between them can be expressed by a derivative, and the intra-layer stress becomes

$$\sigma_{iz}^{\mathrm{int}} = \frac{\zeta}{h}(\partial_z \dot{u}_i), \tag{3}$$

where ζ is the friction coefficient and the dot indicates the time derivative. The above frictional stress arises from, e.g., a viscous fluid between the sheets and can be obtained within the lubrication approximation, as shown in Appendix A. However, we note that Eq. (3) is not limited to such a situation and holds more generally for other layered materials.

Using the above result, we now obtain the equation of motion of a layered material with interlayer friction. We assume that the thickness of each sheet is negligibly small. By combining Eq. (2) and (3), the equation of motion of the layered material is generally given by $\rho\ddot{u}_i = \partial_j\sigma_{ij} + h\partial_z\sigma_{iz}^{\mathrm{int}}$, where ρ is the average areal density. If we neglect the effect of inertia under the condition $\rho L^2\omega/\zeta \ll 1$, where L is the thickness of the layered material, we obtain the following force balance equation:

$$\mu\partial_j^2 u_i + (\mu + \lambda)\partial_i\partial_j u_j + \zeta\partial_z^2\dot{u}_i = 0. \tag{4}$$

As shown in Figure 1, the bottom of the layered material ($z = 0$) is supported by a solid substrate and the

displacement vanishes there. On the other hand, we apply displacement $\mathbf{U}(\mathbf{r},t)$ at the top surface ($z=L$). Hence, the boundary conditions for the displacement field are written as

$$\mathbf{u}(\mathbf{r},z,t)=\begin{cases}0 & \text{at } z=0\\ \mathbf{U}(\mathbf{r},t) & \text{at } z=L\end{cases}. \tag{5}$$

Response Function in the Fourier Space

In this section, we discuss the mechanical response of the layered material described by Eq. (4) under the boundary conditions in Eq. (5). We first introduce the 2D Fourier transform defined by

$$u_i[\mathbf{q},z,\omega]=\int d^2\mathbf{r}\int dt\, u_i(\mathbf{r},z,t)e^{-i(\mathbf{q}\cdot\mathbf{r}+\omega t)}, \tag{6}$$

$$u_i(\mathbf{r},z,t)=\int\frac{d^2\mathbf{q}}{(2\pi)^2}\int\frac{d\omega}{2\pi}\,u_i[\mathbf{q},z,\omega]e^{i(\mathbf{q}\cdot\mathbf{r}+\omega t)}, \tag{7}$$

where $\mathbf{q}=(q_x,q_y)$ is the 2D wavevector and ω is the frequency. Then, the Fourier transform of Eq. (4) becomes

$$\partial_z^2 u_i[\mathbf{q},z,\omega]=A_{ij}[\mathbf{q},\omega]u_j[\mathbf{q},z,\omega], \tag{8}$$

where we have introduced

$$A_{ij}[\mathbf{q},\omega]=\frac{q^2}{i\omega\zeta}\left[\mu\delta_{ij}+(\mu+\lambda)\frac{q_iq_j}{q^2}\right], \tag{9}$$

and $q=|\mathbf{q}|$.

Equation (8) is a second-order linear differential equation that can be solved easily. The eigenvalues $\xi_\pm$ and the corresponding eigenvectors $\mathbf{w}_\pm$ of the matrix A_{ij} are obtained as

$$\xi_+=\frac{q^2}{i\omega\zeta}(2\mu+\lambda),\quad \mathbf{w}_+=\begin{pmatrix}q_x\\ q_y\end{pmatrix}, \tag{10}$$

$$\xi_-=\frac{q^2}{i\omega\zeta}\mu,\qquad \mathbf{w}_-=\begin{pmatrix}q_y\\ -q_x\end{pmatrix}. \tag{11}$$

Then the general solution of $u_i[\mathbf{q},z,\omega]$ is obtained as

$$\mathbf{u}[\mathbf{q},z,\omega]=\begin{pmatrix}q_x & q_y\\ q_y & -q_x\end{pmatrix}\begin{pmatrix}a_1e^{\sqrt{\xi_+}z}+a_2e^{-\sqrt{\xi_+}z}\\ a_3e^{\sqrt{\xi_-}z}+a_4e^{-\sqrt{\xi_-}z}\end{pmatrix}. \tag{12}$$

In the above, $a_1,\ldots,a_4$ are the coefficients determined by the boundary conditions in Eq. (5) and are given by

$$a_1=-a_2=\frac{U_xq_x+U_yq_y}{2q\sinh(\sqrt{\xi_+}L)}, \tag{13}$$

$$a_3=-a_4=\frac{U_xq_y-U_yq_x}{2q\sinh(\sqrt{\xi_-}L)}. \tag{14}$$

The linear response to the applied displacement $\mathbf{U}(\mathbf{r},t)$ at the material surface ($z=L$) can be written in the following way:

$$u_i[\mathbf{q},z,\omega]=\gamma_{ij}[\mathbf{q},z,\omega]U_j[\mathbf{q},\omega]. \tag{15}$$

Here, $\gamma_{ij}[\mathbf{q},z,\omega]$ is the response function in the Fourier space and can be represented as

$$\gamma_{ij}[\mathbf{q},z,\omega]=B_1[\mathbf{q},z,\omega]\delta_{ij}+B_2[\mathbf{q},z,\omega]\frac{q_iq_j}{q^2}. \tag{16}$$

After some calculation, we obtain

$$B_1[\mathbf{q},z,\omega]=F[\tilde{q},\tilde{z},\tilde{\omega}_\perp], \tag{17}$$

$$B_2[\mathbf{q},z,\omega]=F[\tilde{q},\tilde{z},\tilde{\omega}_\parallel]-F[\tilde{q},\tilde{z},\tilde{\omega}_\perp], \tag{18}$$

where the function $F[\tilde{q},\tilde{z},\tilde{\omega}]$ is defined by

$$F[\tilde{q},\tilde{z},\tilde{\omega}]=\frac{\sinh\left[(1-i)\tilde{q}\tilde{z}/\sqrt{\tilde{\omega}}\right]}{\sinh\left[(1-i)\tilde{q}/\sqrt{\tilde{\omega}}\right]}, \tag{19}$$

and the dimensionless quantities are $\tilde{q}=qL$, $\tilde{z}=z/L$, $\tilde{\omega}_\perp=(2\zeta/\mu)\omega$, and $\tilde{\omega}_\parallel=[2\zeta/(2\mu+\lambda)]\omega$. Note that $\tilde{\omega}_\parallel$ and $\tilde{\omega}_\perp$ are related by $\tilde{\omega}_\parallel=(1-\nu)\tilde{\omega}_\perp/2$, where $\nu=\lambda/(2\mu+\lambda)$ is the 2D Poisson ratio. In Eq. (19), the frequency dependence enters only with the combination $\tilde{\omega}/\tilde{q}^2$.

Using the obtained response function, we discuss the internal displacement of the layered material. Owing to the 2D isotropy, we set here $U_y=0$ for simplicity and without loss of generality. If we apply a transverse displacement $U_x\sim e^{i(qy+\omega t)}$ at $z=L$, the internal displacement is given by $u_x[\mathbf{q},z,\omega]=B_1=F[\tilde{q},\tilde{z},\tilde{\omega}_\perp]$ according to Eq. (15) and (16). For a longitudinal displacement $U_x\sim e^{i(qx+\omega t)}$ at $z=L$, on the other hand, the internal displacement is given by $u_x[\mathbf{q},z,\omega]=B_1+B_2=F[\tilde{q},\tilde{z},\tilde{\omega}_\parallel]$. Hence, the internal displacement is essentially expressed by the function $F[\tilde{q},\tilde{z},\tilde{\omega}]$ in Eq. (19) both for the transverse and longitudinal surface displacements at $z=L$.

Let us look at the asymptotic behaviors of the function $F[\tilde{q},\tilde{z},\tilde{\omega}]$. In the limit of $\tilde{\omega}\gg\tilde{q}^2$, Eq. (19) becomes

$$F[\tilde{q},\tilde{z},\tilde{\omega}]\approx\tilde{z}. \tag{20}$$

This means that the displacement is linearly transmitted through the layered material. In the limit of $\tilde{\omega}\ll\tilde{q}^2$ and $\tilde{z}\approx 1$, we have

$$F[\tilde{q},\tilde{z},\tilde{\omega}]\approx\exp\left[(1-i)\tilde{q}(\tilde{z}-1)/\sqrt{\tilde{\omega}}\right]. \tag{21}$$

This expression indicates that $\sqrt{\tilde{\omega}}/\tilde{q}$ corresponds to the screening length beyond which the displacement decays out.

In Figure 2, we plot the function $F[\tilde{q}, \tilde{z}, \tilde{\omega}]$ as a function of $\tilde{z}$ for $\tilde{\omega}/\tilde{q}^2 = 0.2$, 0.5, and 1. Since F is a complex quantity and can be written as $F = |F|e^{i(\arg F)}$, we plot its absolute value $|F|$ and the argument $(\arg F)$ in (a) and (b), respectively. In Figure 2(a), we see that $|F|$ interpolates between 0 and 1 in a nonlinear manner, and it is smaller when $\tilde{\omega}/\tilde{q}^2$ is smaller. This means that the displacement at $z = L$ cannot be transmitted deep into the layered material when the frequency is small. In Figure 2(b), we see that the transmission of the displacement is delayed when $\tilde{\omega}/\tilde{q}^2$ is smaller. This is because each sheet undergoes different displacements with different phases when the frequency is small. When the argument of F is close to π or $-\pi$, the phase is completely opposite to the applied displacement at $z = L$.

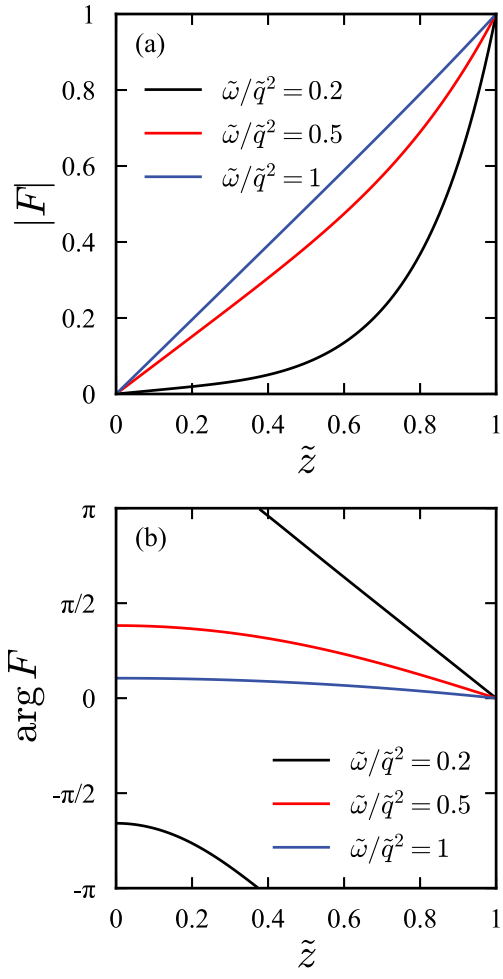

Figure 2. The plots of (a) the absolute value and (b) the argument of the complex function $F[\tilde{q}, \tilde{z}, \tilde{\omega}]$ in Eq. (19) as a function of $\tilde{z} = z/L$ for $\tilde{\omega}/\tilde{q}^2 = 0.2$, 0.5, and 1.

Response Function in the Real Space

Using the Fourier space response function in Eq. (16), we now obtain the response function in the real space. In the real space, Eq. (15) can be written as

$$u_i(\mathbf{r}, z, \omega) = \int d^2\mathbf{r}' \, \Gamma_{ij}(\mathbf{r} - \mathbf{r}', z, \omega) U_j(\mathbf{r}', \omega), \tag{22}$$

where

$$\Gamma_{ij}(\mathbf{r}, z, \omega) = \int \frac{d^2\mathbf{q}}{(2\pi)^2} \gamma_{ij}[\mathbf{q}, z, \omega] e^{i\mathbf{q}\cdot\mathbf{r}}. \tag{23}$$

Due to the symmetry property $\Gamma_{ij} = \Gamma_{ji}$, we can write the response function in the form

$$\Gamma_{ij}(\mathbf{r}, z, \omega) = C_1(r, z, \omega)\delta_{ij} + C_2(r, z, \omega)\frac{r_i r_j}{r^2}, \tag{24}$$

where $r = |\mathbf{r}|$. In the above, C_1 and C_2 are obtained by calculating Γ_{ii} and $\Gamma_{ij} r_i r_j / r^2$. From Eq. (16) and (23), the integral forms of C_1 and C_2 are

$$C_1(\tilde{r}, \tilde{z}, \tilde{\boldsymbol{\omega}}) = \frac{1}{2\pi L^2} \int_0^\infty d\tilde{q}\,\tilde{q} \Big[J_0(\tilde{q}\tilde{r}) B_1[\tilde{q}, \tilde{z}, \tilde{\boldsymbol{\omega}}] + \left(J_0(\tilde{q}\tilde{r}) - \frac{J_1(\tilde{q}\tilde{r})}{\tilde{q}\tilde{r}} + J_2(\tilde{q}\tilde{r}) \right) B_2[\tilde{q}, \tilde{z}, \tilde{\boldsymbol{\omega}}] \Big], \tag{25}$$

$$C_2(\tilde{r}, \tilde{z}, \tilde{\boldsymbol{\omega}}) = \frac{1}{2\pi L^2} \int_0^\infty d\tilde{q}\,\tilde{q} \Big[-J_0(\tilde{q}\tilde{r}) + \frac{2J_1(\tilde{q}\tilde{r})}{\tilde{q}\tilde{r}} - 2J_2(\tilde{q}\tilde{r}) \Big] B_2[\tilde{q}, \tilde{z}, \tilde{\boldsymbol{\omega}}], \tag{26}$$

where $J_n(x)$ is the Bessel function of the first kind and $\tilde{r} = r/L$. These integrals can be numerically performed by using Mathematica.

Having obtained the response function Γ_{ij} in the real space, we discuss here its longitudinal and transverse components. Given the surface deformation $\mathbf{U}(\mathbf{r}, \omega) = \mathbf{U}(\omega)\delta(\mathbf{r})$ at $z = L$, we obtain the internal displacement $\mathbf{u}(r, z, \omega)$. If we choose the x-axis to be the direction of the applied surface displacement at $z = L$, one can consider the longitudinal response $\Gamma_{xx} = C_1 + C_2$ and the transverse response $\Gamma_{yy} = C_1$ as before.

In Figures 3(a) and (b), we plot the absolute value and the argument of complex Γ_{xx}, respectively, as a function of $\tilde{r}$ for $\tilde{z} = 0.75$, 0.5, and 0.25. We see that $|\Gamma_{xx}|$ monotonically decreases as $\tilde{r}$ increases. More precisely, $|\Gamma_{xx}|$ decreases as $-r^2$ for $\tilde{r} \ll 1$ while it decays as r^{-3} for $\tilde{r} \gg 1$, as derived in

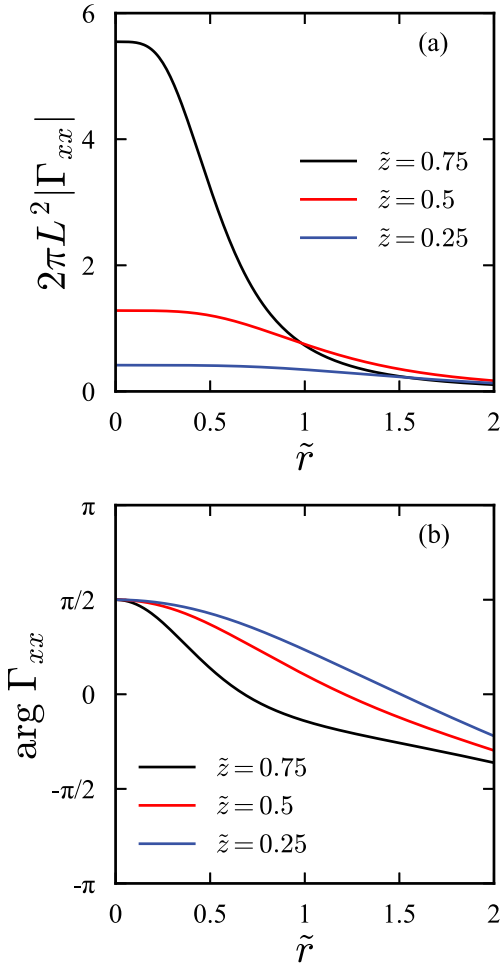

Figure 3. The plots of (a) the absolute value and (b) the argument of the complex function $\Gamma_{xx}(\mathbf{r}, z, \omega)$ in Eq. (24) as a function of $\tilde{r} = r/L$ for $\tilde{z} = 0.25$, 0.5, and 0.75. The other parameters are $\tilde{\omega}_\perp = 1$ and $\nu = 1/6$.

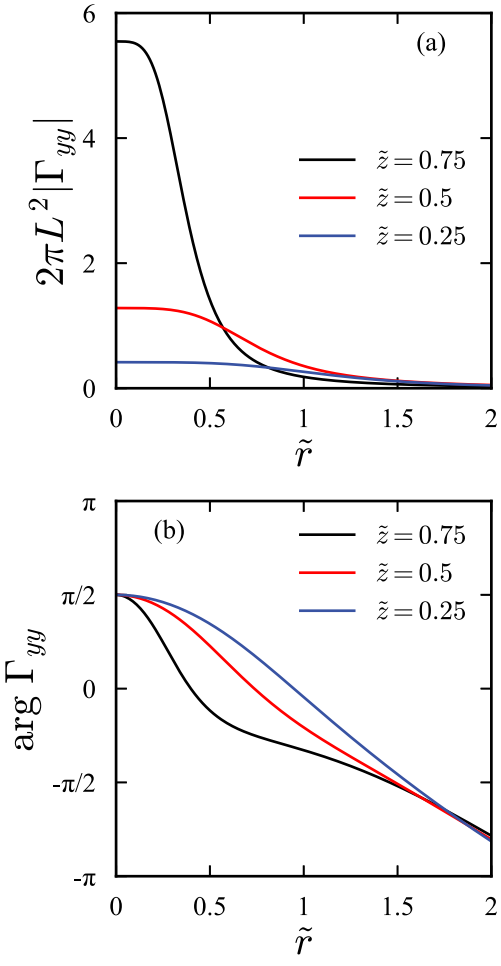

Figure 4. The plots of (a) the absolute value and (b) the argument of the complex function $\Gamma_{yy}(\mathbf{r}, z, \omega)$ in Eq. (24) as a function of $\tilde{r} = r/L$ for $\tilde{z} = 0.25$, 0.5, and 0.75. The other parameters are $\tilde{\omega}_\perp = 1$ and $\nu = 1/6$.

Appendix B. In Figure 3(b), we see that the argument of Γ_{xx} is $\pi/2$ at $\tilde{r} = 0$, indicating that the displacement at $z = L$ is transmitted through the interlayer friction for $\tilde{r} = 0$. When $\tilde{r}$ is further increased, the argument of Γ_{xx} monotonically decreases even to negative values. In Figures 4(a) and (b), we plot the absolute value and the argument of Γ_{yy}, respectively, as a function of $\tilde{r}$ for $\tilde{z} = 0.75$, 0.5, and 0.25. Although the behavior of Γ_{yy} is similar to that of Γ_{xx}, the transverse response Γ_{yy} decays slightly faster than Γ_{xx}.

Effective Complex Modulus

For the layered material shown in Figure 1, we define an effective complex modulus $G^*[\mathbf{q}, \omega]$ by using the stress σ^L_{xz} at $z = L$ and σ^0_{xz} at $z = 0$ as

$$\frac{1}{2}\left(\sigma^L_{xz}[\mathbf{q}, \omega] + \sigma^0_{xz}[\mathbf{q}, \omega]\right) = \frac{1}{L} G^*[\mathbf{q}, \omega] U_x[\mathbf{q}, \omega]. \quad (27)$$

Here we have set $U_y = 0$ and use Eq. (3) and (15) to obtain

$$\sigma^{L,0}_{xz}[\mathbf{q}, \omega] = \frac{i\omega\zeta}{h} \partial_z \gamma_{xx}[\mathbf{q}, z, \omega]|_{z=L,0} U_x[\mathbf{q}, \omega]. \quad (28)$$

Since γ_{xx} in Eq. (16) is essentially given by $F[\tilde{q}, \tilde{z}, \tilde{\omega}_\perp]$ in Eq. (19) for the transverse surface displacement, the effective modulus $G^*[\mathbf{q}, \omega]$ is obtained as

$$G^*[\mathbf{q}, \omega] = \frac{i\omega\zeta L}{2h}\left(\partial_z F[\tilde{q}, \tilde{z}, \tilde{\omega}_\perp]|_{z=L} + \partial_z F[\tilde{q}, \tilde{z}, \tilde{\omega}_\perp]|_{z=0}\right)$$

$$= \frac{i\omega\zeta(1-i)\tilde{q}}{2h\sqrt{\tilde{\omega}_\perp}}\left[\frac{1}{\tanh\left[(1-i)\tilde{q}/\sqrt{\tilde{\omega}_\perp}\right]} + \frac{1}{\sinh\left[(1-i)\tilde{q}/\sqrt{\tilde{\omega}_\perp}\right]}\right]. \quad (29)$$

The behaviors of the real and imaginary parts of G^* denoted by G' and G'', respectively, are shown in Figure 5.

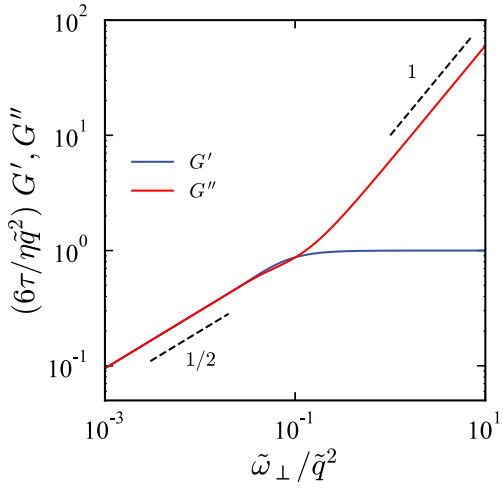

Figure 5. The real part (G') and the imaginary part (G'') of the effective complex modulus $G^*[q,\omega]$ in Eq. (29). The dashed lines represent the asymptotic power-law behaviors in Eqs. (30) and (31).

Let us discuss the asymptotic behaviors of Eq. (29). In the limit of $\tilde{\omega}_\perp \gg \tilde{q}^2$, we have

$$G^*[q,\omega] \approx \frac{i\omega\zeta}{h} + \frac{\zeta\tilde{q}^2}{6h\tau}, \tag{30}$$

where $\tau = 2\zeta/\mu$ is the relaxation time for the transverse surface displacement as we discussed in Section III. The above expression is analogous to the complex modulus of the Kelvin-Voigt model. In the limit of $\tilde{\omega}_\perp \ll \tilde{q}^2$, on the other hand, we have

$$G^*[q,\omega] \approx \frac{\sqrt{2}\zeta\tilde{q}}{2h\tau}(i\tilde{\omega}_\perp)^{1/2}, \tag{31}$$

which is an intermediate power-law behavior. In the long-length limit, however, the layered material behaves as a fluid because $G^* \to i\omega\zeta/h$ for $q \to 0$.

It was experimentally found that the complex modulus of the lamellar phase in diblock copolymers behaves as $G^* \sim (i\omega)^{1/2}$.[11–14] Using the smectic free energy of liquid crystals, Kawasaki and Onuki proposed a theory to describe the intermediate behavior between fluids and solids.[15] Although we obtain a similar frequency dependence in Eq. (31), we do not consider that our result explains the experimental observation in block copolymers because of the following reasons. (i) In the experiment, the anomalous behavior $G^* \sim (i\omega)^{1/2}$ disappears if layers are oriented by application of shear. (ii) The power-law behavior in Eq. (31) appears only for finite q and cannot be a macroscopic response for $q \to 0$.

Summary and Discussion

In this paper, we have discussed the mechanical properties of a layered material with interlayer friction. We have proposed a new model that contains both lateral elasticity and interlayer friction. Considering only the in-plane deformation, we obtained the response function in the Fourier and the real spaces. In particular, we have looked at how the internal displacement is induced by the surface lateral displacement. We find that the applied surface displacement is transmitted into the material with an apparent phase difference due to the interlayer friction. We also obtained the effective complex modulus of the layered material and showed that it exhibits an intermediate power-law behavior in the low-frequency regime. Our model is general and can be applied for various layered materials at different scales ranging from microscopic to macroscopic sizes.

In our model, we have assumed that the 2D sheets are elastic and interlayer friction acts between them. As shown in Appendix A, such a friction can be obtained, for example, within the lubrication approximation for the fluid layer between the elastic sheets. It is also similar to that acting between two leaflets in a fluid bilayer membrane.[31–34] On the other hand, the situation is different in graphene sheets[17,18] or layered viscoelastic materials[19] in which elastic interactions act between the sheets. Since elastic interactions do not lead to any dissipation, the mechanical response should be different from what we have discussed in the paper.

In the present work, we have discussed only the lateral in-plane displacement at the surface of the layered material and investigated how it is transmitted into the material. In the future, we shall also investigate the mechanical response to the out-of-plane surface displacement. For a thin elastic sheet, it is known that in-plane and out-of-plane displacements are coupled to each other so that bending always accompanies stretching.[28] For such a non-linear coupling, one can eliminate the in-plane degrees of freedom, which results in the renormalization of the bending rigidity.[29,30] A hydrodynamic theory for a single polymerized membrane was discussed in Ref. [35] by focusing on the dynamics of out-of-plane deformation that is coupled to the surrounding fluid.

In order to consider the mechanical response to the out-of-plane deformation in the layered material, one needs to further take into account such as the bending rigidity and layer compression modulus that are used to describe the elasticity of the smectic phase in liquid crystals.[36] For multi-layered elastic sheets, the steric interactions between two elastic sheets are very different from those between fluid membranes.[37] Moreover, it is necessary to

investigate the effects of hydrodynamic interactions between elastic sheets for out-of-plane deformation. These extended studies are left for our future work. However, we emphasize that even the lateral response to in-plane deformation appears to be non-trivial due to the friction between the layers, as we have discussed in this paper.

In our previous work on two-layer vesicles,[38] we argued both the bending energy and the stretching energy of the fluid membranes as well as the hydrodynamics of the surrounding fluid. We can also extend this theory to a multi-layer system by including the shear elasticity of each sheet.

Acknowledgments

K.Y. acknowledges the support by a Grant-in-Aid for JSPS Fellows (Grant No. 21J00096) from the Japan Society for the Promotion of Science. K.Y. was supported by the Research Institute for Mathematical Sciences, an International Joint Usage/Research Center located in Kyoto University. S. K. acknowledges the supported by the startup fund of Wenzhou Institute, University of Chinese Academy of Sciences (No. WIUCASQD2021041).

Disclosure Statement

No potential conflict of interest was reported by the author(s).

Funding

This work was supported by the Wenzhou Institute [WIUCASQD2021041]; Grant-in-Aid for JSPS Fellows [21J00096].

ORCID

Kento Yasuda http://orcid.org/0000-0003-4275-775X
Yuto Hosaka http://orcid.org/0000-0002-6202-4206
Shigeyuki Komura http://orcid.org/0000-0003-3422-5745

References

[1] Larson, R. G. *The Structure and Rheology of Complex Fluids*; New York: Oxford University Press, 1999.
[2] Witten, T. A., and Pincus, P. *Structured Fluids: Polymers, Colloids, Surfactants*; New York: Oxford University Press, 2010.
[3] de Gennes, P. G. Dynamics of Entangled Polymer Solutions. I. The Rouse Model. *Macromolecules*. 1976, 9, 587. DOI: 10.1021/ma60052a011.
[4] de Gennes, P. G. Dynamics of Entangled Polymer Solutions. II. Inclusion of Hydrodynamic Interactions. *Macromolecules*. 1976, 9, 594. DOI: 10.1021/ma60052a012.
[5] Colby, R. H.; Ober, C. K.; Gillmor, J. R.; Connelly, R. W.; Duong, T.; Galfi, G.; Laus, M. Rheol. *Acta*. 1997, 36, 498.
[6] Lu, C.-Y. D.; Chen, P.; Ishii, Y.; Komura, S.; Kato, T. Non-linear Rheology of Lamellar Liquid Crystals. *Eur. Phys. J. E*. 2008, 25, 91. DOI: 10.1140/epje/i2007-10267-3.
[7] Fujii, S.; Ishii, Y.; Komura, S.; Lu, C.-Y. D. Smectic Rheology Close to the smectic-nematic Transition. *EPL*. 2010, 90, 64001. DOI: 10.1209/0295-5075/90/64001.
[8] Fujii, S.; Komura, S.; Ishii, Y.; Lu, C.-Y. D. Elasticity of Smectic Liquid Crystals with Focal Conic Domains. *J. Phys. Condens. Matter*. 2011, 23, 235105. DOI: 10.1088/0953-8984/23/23/235105.
[9] Fujii, S.; Komura, S.; Lu, C.-Y. D. Structural Rheology of Focal Conic Domains: A stress-quench Experiment. *Soft Matter*. 2014, 10, 5289. DOI: 10.1039/c4sm00146j.
[10] Fujii, S.; Komura, S.; Lu, C.-Y. D. Structural Rheology of the Smectic Phase. *Materials*. 2014, 7, 5146. DOI: 10.3390/ma7075146.
[11] Fredrickson, G. H.; Bates, F. S. Dynamics of Block Copolymers: Theory and Experiment. *Rev. Mater. Sci*. 1996, 26, 501. DOI: 10.1146/annurev.ms.26.080196.002441.
[12] Bates, F. S.; Rosedale, J. H.; Fredrickson, G. H. Fluctuation Effects in a Symmetric Diblock Copolymer near the order–disorder Transition. *J. Chem. Phys*. 1990, 92, 6255. DOI: 10.1063/1.458350.
[13] Rosedale, J. H.; Bates, F. S. Rheology of Ordered and Disordered Symmetric Poly(ethylenepropylene)-poly(ethylethylene) Diblock Copolymers. *Macromolecules*. 1990, 23, 2329. DOI: 10.1021/ma00210a032.
[14] Bates, F. S. Block Copolymers near the Microphase Separation Transition. 2. Linear Dynamic Mechanical Properties. *Macromolecules*. 1984, 17, 2607. DOI: 10.1021/ma00142a025.
[15] Kawasaki, K.; Onuki, A. Dynamics and Rheology of Diblock Copolymers Quenched into microphase-separated States. *Phys. Rev. A*. 1990, 42, 3664. DOI: 10.1103/PhysRevA.42.3664.
[16] Alberts, B.; Johnson, A.; Lewis, J.; Raff, M.; Roberts, K., and Walter, P. *Molecular Biology of the Cell*; Garland Science, New York, 2008.
[17] Kolahchi, R.; Kolahdouzan, F. A Numerical Method for magneto-hygro-thermal Dynamic Stability Analysis of Defective Quadrilateral Graphene Sheets Using Higher Order Nonlocal Strain Gradient Theory with Different Movable Boundary Conditions. *Appl. Math. Model*. 2021, 91, 458. DOI: 10.1016/j.apm.2020.09.060.
[18] Mehrez, S.; Karati, S. A.; DolatAbadi, P. T.; Shah, S. N. R.; Azam, S.; Khorami, M., and Assilzadeh, H. Nonlocal dynamic modeling of mass sensors consisting of graphene sheets based on strain gradient theory. *Adv. Nano Res*. 2020, 9, 221.
[19] Xu, P.-C.; Mal, A. K. Calculation of the Inplane Green's Functions for a Layered Viscoelastic Solid. *Bull. Seismol. Soc. Am*. 1987, 77, 1823. DOI: 10.1785/BSSA0770051823.
[20] Nallet, F.; Roux, D.; Prost, J. Hydrodynamics of Lyotropic Smectics: A Dynamic Light Scattering Study of Dilute Lamellar Phases. *J. Phys. (France)*. 1989, 50, 3147. DOI: 10.1051/jphys:0198900500200314700.

[21] Nallet, F.; Roux, D.; Quilliet, C.; Fabre, P., and Milner, S. Elasticity and hydrodynamic properties of "doped solvent dilute" lamellar phases. *J. Phys. II (France)*. 1994 , 4, 1477.
[22] Ramaswamy, S.; Prost, J.; Cai, W.; Lubensky, T. C. Dynamics of Lyotropic Lamellar Phases. *Europhys. Lett.* 1993, 23, 271. DOI: 10.1209/0295-5075/23/4/006.
[23] Roux, D.; Nallet, F.; Diat, O. Rheology of Lyotropic Lamellar Phases. *Europhys. Lett.* 1993, 24(53). DOI: 10.1209/0295-5075/24/1/009.
[24] Panizza, P.; Roux, D.; Vuillaume, V.; Lu, C.-Y. D.; Cates, M. E. Viscoelasticity of the Onion Phase. *Langmuir*. 1996, 12, 248. DOI: 10.1021/la9504016.
[25] Bonn, D.; Meunier, J.; Greffier, O.; Al-Kahwaji, A.; Kellay, H. Bistability in non-Newtonian Flow: Rheology of Lyotropic Liquid Crystals. *Phys. Rev. E*. 1998, 58, 2115. DOI: 10.1103/PhysRevE.58.2115.
[26] Zilman, A. G.; Granek, R. Undulation Instability of Lamellar Phases under Shear: A Mechanism for Onion Formation? *Eur. Phys. J. B*. 1999, 11, 593. DOI: 10.1007/s100510051187.
[27] Marlow, S. W.; Olmsted, P. D. Eur. *Phys. J. E*. 2002, 8, 485.
[28] Landau, L. D., and Lifshitz, E. M. *Theory of Elasticity*; New York: Pergamon Press, 1986.
[29] Nelson, D. R., and Peliti, L. Fluctuations in membranes with crystalline and hexatic order. *J. Phys. Paris*. 1987 , 48, 1085.
[30] Doussal, P. L.; Radzihovsky, L. Anomalous Elasticity, Fluctuations and Disorder in Elastic Membranes. *Ann. Phys*. 2018, 392, 340. DOI: 10.1016/j.aop.2017.08.033.
[31] Seifert, U., and Langer, S. Viscous Modes of Fluid Bilayer Membranes. *Europhys. Lett*. 1993 , 23(71).
[32] Okamoto, R.; Kanemori, Y.; Komura, S.; Fournier, J.-B. Relaxation Dynamics of two-component Fluid Bilayer Membranes. *Eur. Phys. J. E*. 2016, 39(52). DOI: 10.1140/epje/i2016-16052-3.
[33] Okamoto, R.; Komura, S.; Fournier, J.-B. Dynamics of a Bilayer Membrane Coupled to a two-dimensional Cytoskeleton: Scale Transfers of Membrane Deformations. *Phys. Rev. E*. 2017, 96, 012416. DOI: 10.1103/PhysRevE.96.012416.
[34] Yasuda, K.; Okamoto, R.; Komura, S.; Fournier, J.-B. Dynamics of a Bilayer Membrane with membrane-solvent Partial Slip Boundary Conditions. *Soft Mater*. 2018, 16, 186. DOI: 10.1080/1539445X.2018.1462830.
[35] Frey, E., and Nelson, D. R. Dynamics of flat membranes and flickering in red blood cells*J. Phys. I (France)*. 1991 , 1, 1715.
[36] de Gennes, P. G., and Prost, J. *The Physics of Liquid Crystals*; New York: Oxford University Press, 1993.
[37] Leibler, S.; Maggs, A. Entropic Interactions between Polymerized Membranes. *Phys. Rev. Lett*. 1989, 63, 406. DOI: 10.1103/PhysRevLett.63.406.
[38] Lu, C.-Y. D.; Komura, S.; Seki, K. Viscoelasticity of two-layer Vesicles in Solution. *Phys. Rev. E*. 2012, 86, 061401. DOI: 10.1103/PhysRevE.86.061401.
[39] Landau, L. D., and Lifshitz, E. M. *Fluid Mechanics*; New York: Pergamon Press, 1959.
[40] Safran, S. A. *Statistical Thermodynamics of Surfaces, Interfaces, and Membranes*; Massachusetts: Addison-Wesley, 1994.

Appendix A: The interlayer friction due to viscous fluid

In this Appendix, we derive Eq. (3) for the situation in which a 3D viscous fluid exists between the elastic sheets. The stress tensor of a 3D incompressible fluid is given by[39]

$$\sigma^{3D}_{\alpha\beta} = -p\delta_{\alpha\beta} + \eta\left(\partial_\alpha v_\beta + \partial_\beta v_\alpha\right), \tag{A1}$$

where p is the 3D pressure, $\mathbf{v}$ is the 3D fluid velocity, η is the 3D shear viscosity, and $\alpha, \beta = x, y, z$. Moreover, we assume that the fluid satisfies the incompressibility condition, $\partial_\alpha v_\alpha = 0$.

To consider the stress acting on each sheet, we apply the lubrication approximation.[40] We denote the thickness of the lubrication layer by h and the velocity at the upper plane by V_x, whereas the velocity on the elastic sheet vanishes. Then the hydrodynamic equations for the thin fluid layer are

$$\partial_z p = 0, \ \eta\partial_z^2 v_x - \partial_x p = 0, \ \partial_x v_x + \partial_z v_z = 0. \tag{A2}$$

In the absence of the pressure gradient $\partial_x p$, the velocity profile is simply given by a Couette flow, i.e., $v_x = V_x z/h$. We regard the average stress between the upper and the bottom planes as the intra-layer stress given by $\sigma^{\rm int}_{xz} = (\sigma^h_{xz} + \sigma^0_{xz})/2 = \eta V_x/h$. When h is small enough, the stress can be expressed by a derivative as in Eq. (3), where ζ/h should be identified as η.

Appendix B: Asymptotic expressions of Eq. (25) and (26)

In this Appendix, we show the derivation of the asymptotic expressions of C_1 and C_2 in Eqs. (25) and (26), respectively. For $\tilde{r} = 0$, the integrals in Eq. (25) and (26) can be performed analytically, and we obtain

$$C_1(\tilde{r} = 0, \tilde{z}, \tilde{\omega}) = \frac{1}{2\pi L^2}\frac{i(\tilde{\omega}_\perp + \tilde{\omega}_\parallel)}{16}\left[\psi'\left(\frac{1-\tilde{z}}{2}\right) - \psi'\left(\frac{1+\tilde{z}}{2}\right)\right], \tag{B1}$$

where $\psi'(x) = d\psi(x)/dx$ with $\psi(x) = \Gamma'(x)/\Gamma(x)$ and $\Gamma(x)$ is the Gamma function. On the other hand, we have $C_2(\tilde{r} = 0, \tilde{z}, \tilde{\omega}) = 0$.

Next, we consider the limit of $\tilde{r} \ll 1$ and the expansion of the Bessel functions around zero to examine the terms of order $\tilde{r}^2$. Then the integrals in Eq. (25) and (26) can be performed analytically as

$$C_1(\tilde{r}, \tilde{z}, \tilde{\omega}) \approx C_1(0, \tilde{z}, \tilde{\omega}) + \frac{1}{2\pi L^2}\frac{3\tilde{r}^2}{32\cdot 16}(3\tilde{\omega}_\perp^2 + \tilde{\omega}_\parallel^2)\left[\zeta_4\left(\frac{1-\tilde{z}}{2}\right) - \zeta_4\left(\frac{1+\tilde{z}}{2}\right)\right], \tag{B2}$$

$$C_2(\tilde{r}, \tilde{z}, \tilde{\omega}] \approx -\frac{1}{2\pi L^2}\frac{3\tilde{r}^2}{32\cdot 8}(\tilde{\omega}_\perp^2 - \tilde{\omega}_\parallel^2)\left[\zeta_4\left(\frac{1-\tilde{z}}{2}\right) - \zeta_4\left(\frac{1+\tilde{z}}{2}\right)\right], \tag{B3}$$

where $\zeta_n(x)$ is the generalized Riemann zeta function defined as

$$\zeta_n(x) = \sum_{k=0}^{\infty}(k+x)^{-n}. \tag{B4}$$

Next, we discuss the case of $\tilde{r} \gg 1$. In this case, the Bessel functions in Eq. (25) and (26) can be expressed as $J_0(x) \sim x^{-1/2}\cos(x - \pi/4)$ but an analytical treatment is impossible. Here we use the approximation in Eq. (21) to obtain

$$C_1(\tilde{r}, \tilde{z}, \tilde{\omega}) \approx \frac{1}{2\pi L^2}\frac{3\sqrt{2}(1-i)(1-\tilde{z})}{4\tilde{r}^3}\frac{1}{\sqrt{\tilde{\omega}_\perp}}, \tag{B5}$$

$$C_2(\tilde{r}, \tilde{z}, \tilde{\omega}) \approx \frac{1}{2\pi L^2}\frac{3\sqrt{2}(1-i)(1-\tilde{z})}{4\tilde{r}^3}\left[\frac{1}{\sqrt{\tilde{\omega}_\parallel}} - \frac{1}{\sqrt{\tilde{\omega}_\perp}}\right]. \tag{B6}$$

In the above, we have used the relation

$$\lim_{x\to\infty}[\cos(3\tan^{-1}(x)/2) + \sin(3\tan^{-1}(x)/2)] = \frac{3}{\sqrt{2x}}. \tag{B7}$$

Hence we see that the response function decays as r^{-3} at long distances.